Kinetics of $F^- + CH_3Cl$ S_N2 Nucleophilic Substitution

Haobin Wang and William L. Hase*

Contribution from the Department of Chemistry, Wayne State University, Detroit, Michigan 48202

Received July 29, 1996[⊗]

Abstract: Statistical theory is used to calculate the $F^- + CH_3Cl \rightarrow FCH_3 + Cl^-$ rate constant versus relative translational energy E_{rel} and CH_3Cl temperature T. The calculations are performed on a potential energy surface derived from MP2 and QCISD(T) *ab initio* calculations with the 6-311++G(2df,2pd) basis set. At best, statistical theory only qualitatively reproduces the dependence of the experimental rate constant on translational energy and temperature. Using the height of the central barrier with respect to the pre-reaction complex as an adjustable parameter, the experimental rate constant at $E_{rel} = 0.9$ kcal/mol and $T = 296$ K may be fit by statistical theory with a central barrier 3 kcal/mol higher than that determined from the QCISD(T) calculation. The calculation of the S_N2 rate constant is insensitive to whether the unified statistical model or standard RRKM branching ratio expression is used. Also, including anharmonicity for the F^-- - -CH_3Cl complex does not affect the calculated rate constant. A comparison of statistical rate constants with parametrized trajectory capture rate constants suggests that, during the entrance channel capture dynamics, the $F^- + CH_3Cl$ relative translation and CH_3Cl rotation motions are strongly and weakly coupled at low and high E_{rel}, respectively.

I. Introduction

The dynamics of simple gas phase S_N2 reactions of the type,

$$X^- + CH_3Y \rightarrow XCH_3 + Y^- \qquad (1)$$

are of considerable interest due to the nonstatistical effects observed in both experimental and theoretical studies.[1−17] More work needs to be done to obtain an understanding of the microscopic mechanisms for these reactions. The extent to which the kinetics of a reaction differ from the predictions of statistical theories depends on the disagreement between the actual dynamics and the basic assumptions inherent in statistical theories. As shown in modern nonlinear dynamics,[18] most dynamical systems can display both regular and chaotic motion, a behavior contradictive to the ergodic hypothesis of statistical mechanics. Even if the phase space region of interest is chaotic, the time required for the dynamics to become statistical may be very long. Thus, intramolecular vibrational energy redistribution (IVR) may occur on a time scale much longer than or comparable to that for the chemical reaction.

The S_N2 reactions depicted in eq 1 are thought to proceed through the X^-- - -CH_3Y and XCH_3- - -Y^- ion-dipole complexes.[19] For experiments carried out at low pressures, deviations from the predictions of statistical theories may be expected, if IVR is inefficient and microcanonical ensembles are not prepared for the two complexes.[20] At high pressures, due to frequent inelastic collisions of the reacting molecules, canonical ensembles may be prepared for the complexes and a thermally averaged statistical theory may be appropriate for calculating the S_N2 rate constant. Therefore, caution is required when considering nonstatistical effects for S_N2 reactions. Statistical theory calculations need to be performed for the same conditions as used in the experiment.

To provide more insight into comparisons of statistical rate theories and experiments for S_N2 reactions, calculations of the kinetic energy and temperature dependencies of the rate constant for

$$F^- + CH_3Cl \rightarrow FCH_3 + Cl^- \qquad (2)$$

are reported here. The rate constants were measured at low pressures of 0.4−0.5 Torr.[21−23] A trajectory calculation performed for this reaction[24] shows that the lifetimes of the F^-- - -CH_3Cl and FCH_3- - -Cl^- complexes are very short and, thus, do not undergo deactivating collisions at the above pressures, which correspond to collision frequencies of approximately 10^7 s^{-1}. The experimental rate constants have been interpreted with a theoretical model that neglects any influences of the central barrier and, instead, is based on ion−molecule capture modified by an orientation effect.[23] The assumption

[⊗] Abstract published in *Advance ACS Abstracts,* March 15, 1997.

(1) Graul, S. T.; Bowers, M. T. *J. Am. Chem. Soc.* **1991**, *113*, 9696.
(2) Graul, S. T.; Bowers, M. T. *J. Am. Chem. Soc.* **1994**, *116*, 3875.
(3) Viggiano, A. A.; Paschkewitz, J. S.; Morris, R. A.; Paulson, J. F.; Gonzalez-Lafont, A.; Truhlar, D. G. *J. Am. Chem. Soc.* **1991**, *113*, 9404.
(4) Viggiano, A. A.; Morris, R. A.; Paschkewitz, J. S.; Paulson, J. F. *J. Am. Chem. Soc.* **1992**, *114*, 10477.
(5) Basilevsky, M. V.; Ryaboy, V. M. *Chem. Phys. Lett.* **1986**, *129*, 71.
(6) Ryaboy, V. M. *Chem. Phys. Lett.* **1989**, *159*, 371.
(7) Ryaboy, V. M. In *Advances in Classical Trajectory Methods, Vol. 2, Dynamics of Ion−Molecule Complexes*; Hase, W. L., Ed.; JAI Press: Greenwich, CT, 1993; p 115.
(8) Vande Linde, S. R.; Hase, W. L. *J. Am. Chem. Soc.* **1989**, *111*, 2349.
(9) Vande Linde, S. R.; Hase, W. L. *J. Phys. Chem.* **1990**, *94*, 2778.
(10) Vande Linde, S. R.; Hase, W. L. *J. Phys. Chem.* **1990**, *94*, 6148.
(11) Vande Linde, S. R.; Hase, W. L. *J. Chem. Phys.* **1990**, *93*, 7962.
(12) Cho, Y. J.; Vande Linde, S. R.; Zhu, L. H.; Hase, W. L. *J. Chem. Phys.* **1992**, *96*, 8275.
(13) Hase, W. L.; Cho, Y. J. *J. Chem. Phys.* **1993**, *98*, 8626.
(14) Hase, W. L. *Science* **1994**, *266*, 998.
(15) Wang, H.; Zhu, L.; Hase, W. L. *J. Phys. Chem.* **1994**, *98*, 1608.
(16) Wang, H.; Peslherbe, G. H.; Hase, W. L. *J. Am. Chem. Soc.* **1994**, *116*, 9644.
(17) Peslherbe, G. H.; Wang, H.; Hase, W. L. *J. Chem. Phys.* **1995**, *102*, 5626.
(18) Lichtenberg, A. J.; Lieberman, M. A. *Regular and Chaotic Motion*; Springer-Verlag: New York, 1992.
(19) Olmstead, W. M.; Brauman, J. I. *J. Am. Chem. Soc.* **1977**, *99*, 4219.
(20) Baer, T.; Hase, W. L. *Unimolecular Reaction Dynamics. Theory and Experiments*; Oxford University Press: New York, 1996.
(21) DePuy, C. H.; Gronert, S.; Mullin, A.; Bierbaum, V. M. *J. Am. Chem. Soc.* **1990**, *112*, 8650.
(22) O'Hair, R. A. J.; Davico, G. E.; Hacaloglu, H.; Dang, T. T.; DePuy, C. H.; Bierbaum, V. M. *J. Am. Chem. Soc.* **1994**, *116*, 3609.
(23) Su, T.; Morris, R. A.; Viggiano, A. A.; Paulson, J. F. *J. Phys. Chem.* **1990**, *94*, 8426.
(24) Su, T.; Wang, H.; Hase, W. L. To be submitted for publication.

S0002-7863(96)02622-4 CCC: $14.00

Table 1. Potential Energies for Stationary Points on the $F^- + CH_3Cl \rightarrow Cl^-$ Reaction Path[a]

	PES(F,Cl)[b]	MP2[c]	QCISD[c]	QCISD(T)[c]	CCSD(T)[d]	G2(+)[e]
$F^- + CH_3Cl$	0.00	0.00	0.00	0.00	0.00	0.00
F^-- - -CH_3Cl	−15.83	−15.80	−16.08	−16.56	−15.04	−15.60
saddle point	−11.56	−11.56	−12.48	−13.95	−12.01	−12.62
FCH_3- - -Cl^-	−41.23	−41.20	−44.10	−43.44	−41.63	−41.06
$FCH_3 + Cl^-$	−31.32	−31.32	−34.61	−33.54	−32.41	−31.42

[a] Energies are in kcal/mol and do not include zero-point energies. [b] Analytic potential energy function developed here. [c] *Ab initio* calculations presented here. The basis set is 6-311++G(2df,2pd) and the geometries are optimized at the MP2 level of theory. [d] CCSD(T)/vtz+2 calculations based on CEPA/basis-I optimized geometries; ref 28. The vtz+2 basis set is based on Dunning's valence triple-ζ basis set. It includs two diffuse sets of s, p, and d functions at the halogen centers and one of each at the carbon. Also, there is one set of f functions at each of these atoms. The hydrogen is described by 3s and 2p functions. The vtz+2 basis is slightly larger than the 6-311++G(2df,2pd) basis used for our *ab initio* calculations. Basis-I is based on Huzinaga's exponents and contraction coefficients for the s and p functions of the heavy atoms, and the s functions for hydrogen. It is roughtly equivalent to the 6-311+G** basis. [e] Reference 30.

Table 2. *Ab Initio*[a] and Potential Energy Surface Geometries and Relative Energies for Stationary Points on the Reaction Path[b]

	R_{C-F}	R_{C-Cl}	R_{C-H}	∠Cl−C−H	∠H−C−H	energy
			$F + CH_3Cl$ Reactants			
ab initio	∞	1.778	1.083	108.6	110.3	0.0
PES	∞	1.778	1.085	108.9	110.0	0.0
			F^-- - -CH_3Cl Complex			
ab initio	2.511	1.837	1.077	108.1	110.8	−15.795
PES	2.521	1.831	1.078	108.1	110.8	−15.826
			$[F$- - -CH_3- - -$Cl]^-$ Saddle Point			
ab initio	1.997	2.106	1.069	95.9	119.0	−11.556
PES	1.995	2.108	1.069	96.1	118.9	−11.564
			FCH_3- - -Cl^- Complex			
ab initio	1.413	3.178	1.082	70.9	109.9	−41.197
PES	1.410	3.198	1.082	70.7	109.7	−41.234
			$FCH_3 + Cl^-$ Products			
ab initio	1.383	∞	1.086	71.1	110.0	−31.321
PES	1.383	∞	1.085	70.9	109.8	−31.322

[a] MP2/6-311++G(2df,2pd) calculations. [b] Distances are in angstroms, angles are in degrees, and energies are in kilocalories per mole.

Table 3. *Ab Initio* MP2 and Potential Energy Surface Harmonic Frequencies for Stationary Points on the Reaction Path[a]

mode	*ab initio*	expt[b]	PES(F,Cl
A_1, C−Cl str	769	740	772
E, CH_3 rock	1042	1038	1029
A_1, CH_3 deform.	1397	1383	1490
E, CH_3 deform.	1502	1482	1415
A_1, C−H str	3120	3074	3102
E, C−H str	3232	3166	3230
	F^-- - -CH_3Cl Complex		
E, F^- bend	78		79
A_1, F−C str	174		172
A_1, C−Cl str	612		588
E, CH_3 rock	966		1043
A_1, CH_3 deform.	1277		1396
E, CH_3 deform.	1463		1399
A_1, C−H str	3186		3215
E, C−H str	3317		3361
	Saddle Point		
E, F−C−Cl bend	257		229
A_1, F−C−Cl str	305		306
E, CH_3 rock	1007		1208
A_1, out-of-plane bend	1151		1280
E, CH_3 deform.	1427		1406
A_1, C−H str	3224		3224
E, C−H str	3422		3421
reaction coordinate	501 i		498 i
	FCH_3- - -Cl^- Complex		
E, Cl^- bend	94		92
A_1, C−Cl str	113		115
A_1, F−C str	989		997
E, CH_3 rock	1165		1176
A_1, CH_3 deform.	1446		1627
E, CH_3 deform.	1504		1445
A_1, C−H str	3138		3148
E, C−H str	3255		3280
	$FCH_3 + Cl^-$ Products		
A_1, F−C str	1086	1077	1087
E, CH_3 rock	1211	1207	1170
A_1, CH_3 deform.	1505	1496	1653
E, CH_3 deform.	1521	1514	1441
A_1, C−H str	3097	3046	3107
E, C−H str	3199	3165	3232

[a] Frequency units are cm^{-1}. [b] The experimental CH_3Cl and CH_3F harmonic frequencies are from refs 31 and 32, respectively.

that the central barrier is unimportant arises from the large exothermicity of the reaction, which indicates the potential of the barrier must lie much below that of the reactants.

The statistical rate theory calculations were performed with a general analytic potential energy function developed for S_N2 reactions of the type depicted in reaction 1.[9,15] Parameters for this potential energy function were determined from *ab initio* calculations, which are described in the next section.

II. *Ab Initio* Calculations and Potential Energy Function

Ab initio calculations were performed to determine properties of the minimum energy path (MEP)[9,15] and stationary points for reaction 2. The former were only determined at the MP2[25] level of theory, while QCISD and QCISD(T)[26] calculations were also performed to study the stationary points. The 6-311++G(2df,2pd) basis set was used for all the *ab initio* calculations. Energies, structures, and vibrational frequencies calculated for the stationary points are listed in Tables 1, 2, and 3, respectively. Also included in Table 1 are unpublished CCSD(T)[27] *ab initio* calculations by Seeger and Botschwina[28] and G2(+)[29] *ab initio* results.[30]

The harmonic vibrational frequencies obtained at the MP2 level are very accurate and are less than 4% in error compared with the experimental harmonic frequencies for CH_3Cl[31] and CH_3F.[32] From Table 1 it can be seen that the central barrier height with respect to the pre-reaction well is very sensitive to the level of theory used in the calculation. Including triples in the QCISD calculation lowers the central barrier by approximately 1 kcal/mol with respect to the pre-reaction complex F^-- - -CH_3Cl, a result consistent with the high-level CCSD(T) *ab initio* calculations of Seeger and Botschwina.[28] The QCISD(T) calculation predicts the central barrier to lie approximately

(25) Krishnan, R.; Frisch, M. J.; Pople, J. A. *J. Chem. Phys.* **1980**, *72*, 4244.
(26) Pople, J. A.; Head-Gordon, M.; Raghavachari, K. *J. Chem. Phys.* **1987**, *87*, 5968.
(27) Purvis, G. D.; Bartlett, R. J. *J. Chem. Phys.* **1982**, *76*, 1910.
(28) Seeger, S.; Botschwina, P. Private communication. Seeger, S. Dissertation, Cuvillier Verlag: Göttingen, 1995.
(29) Curtiss, L. A.; Raghavachari, K.; Trucks, G. W.; Pople, J. A. *J. Chem. Phys.* **1991**, *94*, 7221.
(30) Glukhovtsev, M. N.; Pross, A.; Radom, L. *J. Am. Chem. Soc.* **1996**, *118*, 6273.
(31) Duncan, J. L.; Allan, A.; McKean, D. C. *Mol. Phys.* **1970**, *18*, 289.
(32) Giguere, J.; Overend, J. *Spectrochim. Acta* **1976**, *32A*, 241.

Table 4. Non-Switching-Function Potential Energy Surface Parameters for PES(F,Cl)[a]

	CH_3Cl, CH_3F Parameters[b]		
r_{MC}	1.7778, 1.3832 Å	b_θ^{MC}	0.1610, 0.1835 mdyn·Å/rad^4
β_{MC}	1.8308, 2.0298 Å^{-1}	f_ϕ^{MC}	0.7312, 0.9158 mdyn·Å/rad^2
D_{MC}	84.38, 115.7 kcal/mol	a_ϕ^{MC}	−0.2305, −0.2305 mdyn·Å/rad^3
θ_{MC}	109.8330, 110.0204°	F_ϕ^a	1.0
ϕ_{MC}	108.9163, 109.1069°	r_{HC}	1.0850 Å
f_θ^{MC}	0.4865, 0.5545 mdyn·Å/rad^2	β_{HC}	1.9058 Å^{-1}
a_θ^{MC}	−0.1494, −0.1703 mdyn·Å/rad^3	D_{HC}	110.00 kcal/mol
	Complex F^-- - -CH_3Cl Parameters		
r_C	2.5107 Å	A	4655.416 Å^6·kcal/mol
g_C	0.6740 Å	B	1403.114 Å^4·kcal/mol
β_C	1.5570 Å^{-1}	c_ϕ	0.63138288 rad^{-2}
D_C	15.7954 kcal/mol		
	Saddle Point Parameters		
θ_{MAX}	120.0°	a_θ^{MAX}	−0.0813 mdyn·Å/rad^3
f_θ^{MAX}	0.3935 mdyn·Å/rad^2	b_θ^{MAX}	0.0019 mdyn·Å/rad^4
	Complex FCH_3- - -Cl^- Parameters		
r_C	3.1776 Å	A	4655.416 Å^6·kcal/mol
g_C	1.7651 Å	B	1403.114 Å^4·kcal/mol
β_C	1.3478 Å^{-1}	c_ϕ	0.63138288 rad^{-2}
D_C	9.8761 kcal/mol		
	Long-Range Parameters for $F^- + CH_3Cl$		
a_ξ	0.01707734 mdyn·Å/rad^3	D	207.96835 Å^4·kcal/mol
b_ξ	1.64786208 Å^{-2}	ϕ_∞	71.0837°
μ_d	1.87 D		
	Long-Range Parameters for $FCH_3 + Cl^-$		
a_ξ	0.01707734 mdyn·Å/rad^3	D	207.96835 Å^4·kcal/mol
b_ξ	1.64786208 Å^{-2}	ϕ_∞	70.8931°
μ_d	1.85 D		

[a] See ref 15 and its Table 5 for a definition of the parameters. [b] The parameters for CH_3F are listed second. The HC Morse parameters r_{HC}, β_{HC}, and D_{HC} are the same for CH_3Cl and CH_3F.

14 kcal/mol below the reactants. For the CCSD(T) calculation the central barrier is 2 kcal/mol higher with respect to the reactants.

The analytic potential energy function used for $F^- + CH_3Cl \rightarrow FCH_3 + Cl^-$ is identified as PES(F,Cl) and has the same form as that developed previously for the $Cl^- + CH_3Br \rightarrow ClCH_3 + Br^-$ reaction. Parameters for PES(F,Cl) were determined by approximately 1000 MP2 potential energy values calculated for the stationary point geometries, geometries along the MEP, and geometries away from the MEP. MP2 frequencies for statioanry points are also used in the potential function fitting. It would be impractical to calculate this number of potential energy points and perform geometry optimizations and vibrational frequency calculations at the QCISD(T) level of theory with the large 6-311++G(2df,2pd) basis set. In the statistical theory calculations, different values are considered for the central barrier height including the QCISD(T) value. The fitted parameters for PES(F,Cl) are listed in Table 4 and 5. Stationary point properties of PES(F,Cl) are compared with the MP2 stationary point properties in Tables 1−3.

III. Models for Statistical Rate Theory Calculations

Modifications of the unified statistical model[33−35] were used to calculate rate constants for reaction 2 as a function of $F^- + CH_3Cl$ relative translational energy E_{rel} and CH_3Cl temperature T. Transition state theory expresses the thermal rate constant as

$$k(T) = \frac{1}{hQ_r}\int_0^\infty N(E)e^{-E/k_BT}\,dE \qquad (3)$$

where Q_r is the reactant partition function and $N(E)$ is the transition state sum of states, and for simplicity angular momentum is not included in the integral. The unified statistical model extends this expression to reactants with multiple potential energy minima and transition states, by replacing $N(E)$ with

$$N_0(E) = \left[\sum_{k=1,3...}^{2M+1}\frac{1}{N_k(E)} - \sum_{k=2,4...}^{2M}\frac{1}{N_k(E)}\right]^{-1} \qquad (4)$$

where for $k = 1, 3, ..., 2M + 1$ the $\{N_k(E)\}$ are the transition state sums of states and for $k = 2, 4, ..., 2M$ they are the potential minimum sums of states with the reaction coordinate removed. Each sum of states $N_k(E)$ is calculated at a total energy equal to E plus the difference between the potential energy (including the zero-point energy) of the $F^- + CH_3Cl$ reactants and that for the $N_k(E)$ term.

Because of the large reaction exothermicity, the sums of state for the FCH_3- - -Cl^- complex and the FCH_3- - -$Cl^- \leftrightarrow FCH_3 + Cl^-$ variational transition state make negligible contributions to $N_0(E)$ for reaction 2. The $N_k(E)$ which contribute to $N_0(E)$ are $N_{var}^{\ddagger}$ for the $F^- + CH_3Cl \leftrightarrow F^-$- - -$CH_3Cl$ variational transition state, N_{com} for the F^-- - -CH_3Cl complex, and $N_{bar}^{\ddagger}$ for the [F- - -CH_3- - -Cl]$^-$ central barrier. Thus, $N_0(E)$ may be written as

$$N_0(E) = \frac{N_{var}^{\ddagger}(E)N_{bar}^{\ddagger}(E)}{N_{var}^{\ddagger}(E) + N_{bar}^{\ddagger}(E) - N_{var}^{\ddagger}(E)N_{bar}^{\ddagger}(E)/N_{com}(E)} \qquad (5)$$

Inserting this expression into eq 3 gives the unified statistical model's thermal (i.e. canonical) rate constant for reaction 2. The F^-- - -CH_3Cl stretch mode is taken as the reaction coordinate for the F^-- - -CH_3Cl complex and is not included when calculating N_{com}.

The experimental rate constants for reaction 2 are not measured versus temperature, but versus $F^- + CH_3Cl$ relative

(33) Miller, W. H. *J. Chem. Phys.* **1976**, *65*, 2216.
(34) Miller, W. H. In *Potential Energy Surfaces and Dynamics Calculations*; Truhlar, D. G., Ed.; Plenum: New York, 1981; p 265.
(35) Miller, W. H. *J. Phys. Chem.* **1983**, *87*, 3811.

Table 5. Switching-Function Potential Energy Surface Parameters for PES(F,Cl)

switching function[a]	parameter	value
$S_{LR}(g)$, eq 5	C_{LR}	1.68763661
$S_D(g)$, eq 16	a_1	0.491858155
	a_2	0.754712522
	a_3	$1 - a_1 - a_2$
	c_1	0.583384871
	c_2	0.196999118
	c_3	0.750211954
	d_1	3.46199346
	d_2	4.05573320
	d_3	2.25929070
$S_\beta(g_a)$, eq 17	$c_{\beta a}$	0.0309145562
	$n_{\beta a}$[b]	4
$S_\beta(g_b)$, eq 18	$c_{\beta b}$	$0.779184047 \times 10^{-3}$
	$n_{\beta b}$[b]	10
$S_r(g_a)$, eq 19	a_1	0.807352066
	a_2	−0.170837730
	a_3	$1 - a_1 - a_2$
	c_1	1.02764153
	c_2	0.152728140
	c_3	0.182156205
	b_1	1.01708472
	b_2	2.53821373
	b_3	3.99806261
$S_r(g_b)$, eq 20	f_1	1.03177369
	f_2	−0.519496024
	f_3	$1 - f_1 - f_2$
	k_1	0.922957122
	k_2	0.246526197
	k_3	0.0830343589
	h_1	1.13707530
	h_2	2.34587789
	h_3	3.93920183
$S_\phi(g_a)$, eq 24	a_1	−0.258272052
	a_2	0.137438059
	a_3	$1 - a_1 - a_2$
	b_1	0.210452318
	b_2	0.185458511
	b_3	0.0268961675
	g_{0a}	−2.5989
$S_\phi(g_b)$, eq 25	c_1	−0.0351898521
	c_2	−0.532228649
	c_3	$1 - c_1 - c_2$
	d_1	0.0814606547
	d_2	0.0767123252
	d_3	0.0195052139
	g_{0b}	−2.2066
$S_\theta(g)$, eq 26	a_θ	2.30719733
	b_θ	2.17455459
	e_1	2.29782748
	e_2	2.34361005
$S_r(g)$, eq 30	c_r	0.827206135
	$g_r^\ddagger$	−0.3580
$S_\beta(g)$, eq 31	c_β	0.45
	$g_\beta^\ddagger$	−0.1084

[a] The equation number identifies the equation in ref 15 which defines the switching function. [b] This value in the analytic function for $Cl^- + CH_3Br$, ref 15, was set to 3.

translational energy E_{rel} and CH_3Cl temperature T.[23] Thus, eqs 3 and 5 must be modified to account for these experimental conditions and to include orbital and rotational angular momentum effects. A procedure for doing this is identified by considering the situation with a very low central barrier so that $N^\ddagger_{bar}(E) \approx N_{com}(E)$. $N_0(E)$ in eq 5 then becomes equal to $N^\ddagger_{var}(E)$, since $N^\ddagger_{bar}(E) \gg N^\ddagger_{var}(E)$. With $N_0(E) = N^\ddagger_{var}(E)$, the rate constant in eq 3 is that for $F^- + CH_3Cl$ capture. However, for capture with a fixed E_{rel}, fixed CH_3Cl rotational angular momentum quantum numbers j and j_z, and specific quanta **n** in the CH_3Cl vibrational modes, it is inappropriate to use a microcanonical distribution to calculate $N^\ddagger_{var}(E)$. This is because the CH_3Cl vibrational degrees of freedom do not couple statistically with $F^- + CH_3Cl$ relative translation. Instead, the vibrations probably behave adiabatically during capture. Allowing the relative translation and vibrational degrees of freedom to couple statistically would overestimate $N^\ddagger_{var}(E)$ for capture. However, once the F^-- - -CH_3Cl complex is formed relative translation and vibration are assumed to couple statistically, and $N^\ddagger_{var}$ and $N^\ddagger_{bar}$ for decomposition of the complex are determined from microcanonical distributions.

The statistical theory S_N2 rate constant $k_{S_N2}(E_{rel},T)$ for reaction 2, as a function of E_{rel} and CH_3Cl temperature T, is determined by combining the $F^- + CH_3Cl \rightarrow F^-$- - -$CH_3Cl$ capture rate constant with the probability that the F^-- - -CH_3Cl complex dissociates to $FCH_3 + Cl^-$. The approach we use for determining $k_{S_N2}(E_{rel},T)$ is similar to, but has more microscopic detail than, those used previously by Wladkowski et al.,[36] Graul and Bowers,[2] and Wang and Hase.[37] It is assumed the $F^- + CH_3Cl \rightarrow F^-$- - -$CH_3Cl$ capture rate constant $k_{cap}(E_{rel},T)$ is independent of the CH_3Cl vibrational quanta **n** and may, thus, be written as

$$k_{cap}(E_{rel},T) = \sum_{j=0}^{\infty} k_{cap}(E_{rel},j)P(j) \tag{6}$$

where j is the dipole's rotational angular momentum quantum number and $P(j)$ is the probability of j. If the probability of forming the F^-- - -CH_3Cl complex is independent of orbital angular momentum quantum number l and equals unity for l between 0 and l_{max},[37] $k_{S_N2}(E_{rel},T)$ may be represented by combining $k_{cap}(E_{ref},j)$ in eq 6 with the probability $P_{bran}(E,J)$ that once the F^-- - -CH_3Cl complex is formed it dissociates to $FCH_3 + Cl^-$; i.e.

$$k_{S_N2}(E_{rel},T) = \sum_{j=0}^{\infty}\sum_{j=-j}^{j} k_{cap}(E_{rel},j)P(j,j_z)\sum_{l=0}^{l_{max}} P(l)\sum_{n=0}^{\infty} P(n)\sum_{j=|l-j|}^{l+j} P(J)P_{bran}(E,J) \tag{7}$$

The unified statistical model's representation of $P_{bran}(E,J)$ is given by the right-hand side of eq 5 with $N^\ddagger_{var}(E)$ removed from the numerator and the total angular momentum quantum number J included in the remaining sums of states; i.e.

$$P_{bran}(E,J) = \frac{N^\ddagger_{bar}(E,J)}{N^\ddagger_{var}(E,J) + N^\ddagger_{bar}(E,J) - N^\ddagger_{var}(E,J)N^\ddagger_{bar}(E,J)/N_{com}(E,J)} \tag{8}$$

where $E = E_{rel} + E_{rot} + E_{vib}$ is the total energy. The normalized probability distributions $P(l)$, $P(j,j_z)$, $P(\mathbf{n})$, and $P(J)$, for the orbital angular momentum quantum number, the CH_3Cl rotational quantum numbers, the CH_3Cl vibrational quanta, and the total angular momentum quantum numbers, respectively, have been given previously[37] and are not repeated here.

Values of $k_{cap}(E_{rel},j)$ in eq 7 may be deduced from $k_{cap}(E_{rel},T)$, determined from trajectory calculations for an ion and linear rotor colliding with an ion-dipole/ion-induced-dipole potential.[38,39] Su's[38] parametrized expression for $k_{cap}(E_{rel},T)$ is used here. Our initial thought for obtaining $k_{cap}(E_{rel},j)$ was to invert eq 6. However, eq 6 represents the discretized version of the

(36) Wladkowski, B. D.; Lim, K. F.; Allen, W. D.; Brauman, J. I. *J. Am. Chem. Soc.* **1992**, *114*, 9136.
(37) Wang, H.; Hase, W. L. *J. Am. Chem. Soc.* **1995**, *117*, 9347.
(38) Su, T. *J. Chem. Phys.* **1994**, *100*, 4703.
(39) Troe, J. *J. Chem. Phys.* **1996**, *105*, 6249.

inhomogeneous Fredholm equation of the first kind.[40] These equations are often extremely ill-conditioned and the solutions are not unique. Specialized methods have been developed for inverting such equations. However, they must be augmented by additional information regarding the nature of the solution, e.g., the linear and higher-order regularization methods.[40] Since Su's $k_{cap}(E_{rel},T)$ is a parametrized result, the nature of the resulting $k_{cap}(E_{rel},j)$ is not clear. Biased regularization might face the danger of losing the correct physical picture of $k_{cap}(E_{rel},j)$. Even if an accurate numerical value of $k_{cap}(E_{rel},j)$ is found using the kernel of $P(j)$ to reproduce eq 6, one cannot be certain that the $k_{cap}(E_{rel},j)$ is correct for the statistical theory expression, eq 7.

In this work a statistical model with empirical scaling to Su's[38] $k_{cap}(E_{rel},T)$ is used to obtain $k_{cap}(E_{rel},j)$. The statistical calculations are performed for an ion-linear rotor Hamiltonian with an ion-dipole/ion-induced-dipole potential, and are described in the Appendix. It is probably a very good approximation to model CH_3Cl as a linear rotor, since the moment of inertia and, thus, density of states are significantly smaller for the symmetry axis than for the other two rotational axes.

Two approximations were made to eq 7 to determine how they affect $k_{S_N2}(E_{rel},T)$. For the first, the following often applied[36,37] RRKM-type expression for $P_{bran}(E,J)$ was used in eq 7:

$$P_{bran}(E,J) = \frac{N^{\ddagger}_{bar}(E,J)}{N^{\ddagger}_{var}(E,J) + N^{\ddagger}_{bar}(E,J)} \tag{9}$$

The second approximation involved neglecting the j-dependence of the capture rate constant in eq 7 and, thus, expressing the S_N2 rate constant as

$$k_{S_N2}(E_{rel},T) = k_{cap}(E_{rel},T) \sum_{j=0}^{\infty} \sum_{j_z=-j}^{j} P(j,j_z) \sum_{l=0}^{l_{max}} P(l) \sum_{n=0}^{\infty} P(n) \sum_{J=|l-j|}^{l+j} P(J) P_{bran}(E,J) \tag{10}$$

where $P_{bran}(E,J)$ is represented by eq 8. In previous work,[37] eqs 9 and 10 were combined to calculate $k_{S_N2}(E_{rel},T)$ for the $Cl^- + CH_3Br \rightarrow ClCH_3 + Br^-$ reaction. Since the probability distributions in eqs 7 and 10 are the same, both equations equate $k_{S_N2}(E_{rel},T)$ to $k_{cap}(E_{rel},T)$ if $P_{bran}(E,J)$ equals unity. Equation 9 and an equation similar to eq 10 have been used in average dipole orientation/RRKM theory and microcanonical variational transition state/RRKM theory calculations of $k_{S_N2}(E_{rel},T)$ for reaction 2[2] and $ClCH_2CN + Cl^-$,[36] respectively.

The sums of state $N^{\ddagger}_{bar}(E,J)$, $N^{\ddagger}_{var}(E,J)$, and $N_{com}(E,J)$ in eqs 8 and 9 were first calculated with a rigid-rotor/harmonic-oscillator model, treating the K quantum number as an active degree of freedom;[41−43] i.e.

$$N^{\ddagger}(E,J) = \sum_{K=-J}^{J} N^{\ddagger}(E,J,K) \tag{11}$$

The sums $N^{\ddagger}_{bar}(E,J)$ and $N_{com}(E,J)$ were evaluated at the stationary points for the $[F\text{- - -}CH_3\text{- - -}Cl]^-$ barrier and $F^-\text{- - -}CH_3Cl$ complex, respectively. The sum $N^{\ddagger}_{var}(E,J)$ was equated to the minimum in the sum of states along the reaction path.[44−46] Harmonic frequencies were calculated for the vibrational modes orthogonal to the reaction coordinate.[47−49]

Because of the low energies in the variational transition state, anharmonicity is unimportant for $N^{\ddagger}_{var}(E,J)$ and the $N^{\ddagger}_{var}(E,J)$ calculated from eq 11, when Boltzmann averaged, give canonical rate constants for the dissociation of S_N2 ion−molecule complexes nearly equal[15] to those determined for the flexible transition state model,[50,51] the statistical adiabatic channel model,[52,53] the trajectory capture model,[54,55] and the classical variational transition state model.[54] On the other hand, a calculation for the $Cl^-\text{- - -}CH_3Cl$ complex[17] indicates that anharmonicity will increase the sum of states for the $F^-\text{- - -}CH_3Cl$ complex by a factor of 2, which is used here to correct the above anharmonic values for $N_{com}(E,J)$. The effect of not including this correction is considered below, when comparing the calculated and experimental $k_{S_N2}(E_{rel},T)$ for $F^- + CH_3Cl$. Since the transition state at the central barrier has less energy than the $F^-\text{- - -}CH_3Cl$ complex and is also tighter with higher frequencies, a smaller anharmonic correction is expected for the central barrier transition state than for the complex. Thus, for the calculations reported here an anharmonic correction is not included for $N^{\ddagger}_{bar}(E,J)$. In future work it would be of interest to calculate an accurate anharmonic correction for $N^{\ddagger}_{bar}(E,J)$ and determine whether it has an energy dependence which contributes to $k_{S_N2}(E_{rel},T)$.

Anharmonic corrections are not included here in calculating zero-point energies from the harmonic frequencies. Since there is very little shifting of the frequencies in going from $F^- + CH_3Cl$ to the $F^-\text{- - -}CH_3Cl$ complex, anharmonic effects in the zero-point energy are expected to almost cancel between the $F^- + CH_3Cl$ variational transition state and the complex. Anharmonicity will influence the zero-point energy difference between the central barrier and the complex. However, in the following the central barrier height is used as an adjustable parameter to fit the experimental rate constants and the resulting barrier height should be viewed as the classical barrier height, plus the difference in anharmonic zero-point energies between the barrier and complex.

IV. Comparison of Experimental and Calculated $k(E_{rel},T)$

The kinetic energy and temperature dependencies of the $F^- + CH_3Cl$ S_N2 rate constant, determined from the unified statistical model [i.e. eqs 7 and 8], are plotted in Figures 1 and 2. The calculations are based on the analytic potential energy surface PES(F,Cl) described in Section II, with different values for the central barrier height with respect to the pre-reaction complex's potential minimum. In Figure 1, the calculated results are for the MP2 classical central barrier of 4.24 kcal/mol. Including the PES(F,Cl) harmonic zero-point energy difference between the barrier and complex gives a total barrier

(40) Delves, L. M. *Computational Methods for Integral Equations*; Cambridge University Press: New York, 1985.
(41) Aubanel, E. E.; Wardlaw, D. M.; Zhu, L.; Hase, W. L. *Int. Rev. Phys. Chem.* **1991**, *10*, 249.
(42) Zhu, L.; Chen, W.; Hase, W. L.; Kaiser, E. W. *J. Phys. Chem.* **1993**, *97*, 311.
(43) Zhu, L.; Hase, W. L. *Chem. Phys. Lett.* **1990**, *175*, 117.
(44) Truhlar, D. G.; Hase, W. L.; Hynes, J. T. *J. Phys. Chem.* **1983**, *87*, 2664.
(45) Truhlar, D. G.; Garrett, B. C. *Acc. Chem. Res.* **1980**, *13*, 440.
(46) Hase, W. L. *J. Chem. Phys.* **1976**, *64*, 2442.
(47) Miller, W. H.; Handy, N. C.; Adams, J. E. *J. Chem. Phys.* **1980**, *72*, 99.
(48) Fukui, K. *J. Phys. Chem.* **1970**, *74*, 4161.
(49) Fukui, K.; Kato, S.; Fuijmoto, H. *J. Am. Chem. Soc.* **1975**, *97*, 1.
(50) Wardlaw, D. M.; Marcus, R. A. *J. Phys. Chem.* **1986**, *90*, 5383.
(51) Klippenstein, S. J. *J. Chem. Phys.* **1991**, *94*, 6469.
(52) Troe, J. *Chem. Phys. Lett.* **1985**, *122*, 425.
(53) Troe, J. *Chem. Phys.* **1987**, *87*, 2773.
(54) Chesnavich, W. J.; Su, T.; Bowers, M. T. *J. Chem. Phys.* **1980**, *72*, 2641.
(55) Su, T.; Chesnavich, W. J. *J. Chem. Phys.* **1982**, *76*, 5183.

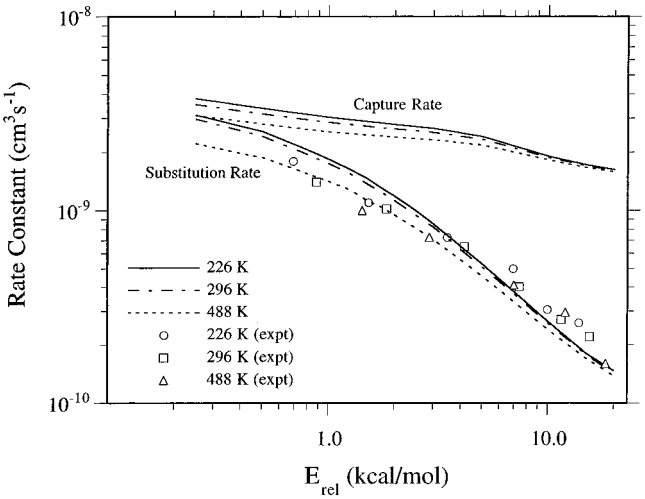

Figure 1. Rate constants for $F^- + CH_3Cl$ S_N2 reaction versus relative translational energy E_{rel} and CH_3Cl internal temperature. The central barrier height is 4.53 kcal/mol with respect to the F^-- - -CH_3Cl pre-reaction complex. This is the MP2/6-311++G(2df,2pd) zero-point corrected central barrier height.

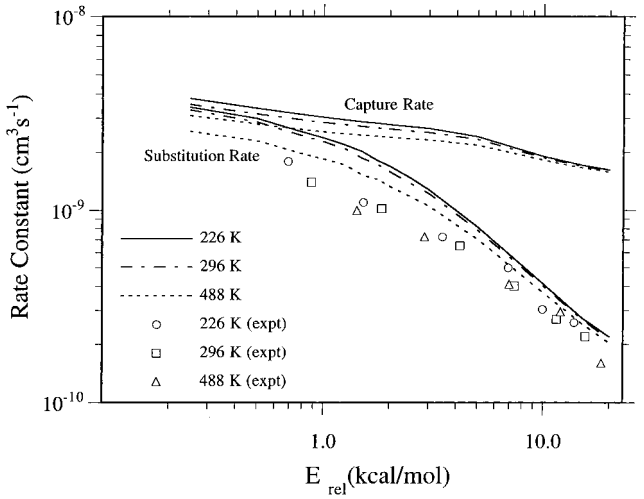

Figure 2. Same as Figure 1, except the barrier height is 2.90 kcal/mol, the QCISD(T)/6-311++G(2df,2pd) zero-point corrected barrier height.

height of 4.53 kcal/mol (The harmonic MP2 frequencies give 0.013 for this zero-point difference). For the calculations in Figure 2, the central barrier height is 2.90 kcal/mol, which is the QCISD(T) classical central barrier height of 2.61 kcal/mol plus the PES(F,Cl) zero-point energy difference. Also plotted in these figures are the experimental rate constants and Su's parametrized $k_{cap}(E_{rel},T)$.

The calculations with the MP2 barrier height semiquantitatively reproduce the experimental kinetic energy dependence of the rate constants. For the QCISD(T) barrier height, the rate constants are higher than the experimental values, but the calculated kinetic energy dependence of the rate constants is still in reasonable agreement with experiment. However, there are distinct differences between the experimental and calculated rate constants. The calculated rate constants decrease more rapidly with increase in E_{rel} than do the experimental ones. Experiment also shows that the rate constants are not distinguishable under different temperatures, while the statistical theory calculations show that the rate constant decreases with increasing temperature. The experimental data (see Figure 1 or 2) are suggestive of slightly smaller rate constants for 488 K than for 226 and 296 K, the trend observed in the calculations. However, this is not a definitive experimental trend and at best seems smaller than that in the statistical theory calculations. For the $Cl^- + CH_3Br$ S_N2 reaction, the experimental rate constants are also independent of temperature, while the statistical theory rate constants are temperature dependent.[37]

Figures 1 and 2 show there are significant differences between the trajectory capture rate constants and those of the unified statistical model. As the kinetic energy increases, the difference between the two sets of rate constants becomes larger. Thus, the low central barrier does not necessarily mean that it cannot serve as a "bottleneck" for the reaction. Due to the tight structure of the central barrier, its moments of inertia are small and, thus, create a high rotational barrier for large total angular momentum. Therefore, whether the central barrier may be neglected depends on the total energy and angular momentum in the statistical theory calculation.

In previous work,[3,37,56] a central barrier height for the $Cl^- + CH_3Br$ S_N2 reaction was estimated by fitting the experimental 300 K rate constant with a statistical theory. The same approach is used here for the $F^- + CH_3Cl$ S_N2 reaction. The experimental data point that is fit is for $E_{rel} = 0.9$ kcal/mol at $T = 296$ K (see Figure 1). To fit this data point with the unified statistical model, eqs 7 and 8, requires a zero-point corrected central barrier height of 5.7 kcal/mol with respect to the pre-reaction complex, which is 1.2 kcal/mol higher than the zero-point corrected MP2 classical barrier. Using this higher barrier has the effect of decreasing the rate constants, shown in Figure 1, calculated with the MP2 barrier. As discussed in Section III, the unified statistical calculation performed for this fit includes a factor of 2 anharmonic correction for the F^-- - -CH_3Cl complex's sums of states. The rate constant does not change within the numerical uncertainty, if this anharmonic correction is removed.

Values for the zero-point corrected central barrier height, with respect to the pre-reaction complex, were also determined by fitting the $E_{rel} = 0.9$ kcal/mol and $T = 296$ K data point with the two approximations to the statistical rate constant. Using the modified unified statistical model, eq 10, with the J-dependence of k_{cap} neglected, has only a minor effect on the fit to this data point and the shape of the $k_{S_N2}(E_{rel},T)$ curves. A slightly smaller zero-point corrected central barrier height of 5.6 kcal/mol is required, instead of the above barrier height of 5.7 kcal/mol fitted with the complete unified statistical model of eqs 7 and 8. On the other hand, using the RRKM-type $P_{bran}(E,J)$ of eq 19 in eq 7, instead of the unified statistical model's P_{bran}, gives the same (within the numerical uncertainty) barrier height of 5.7 kcal/mol. These fitted barrier heights are insensitive to the anharmonic correction for $N_{com}(E,J)$.

As discussed above, the fitted classical central barrier is 1.2 kcal/mol higher than the MP2 classical barrier. Thus from the MP2 energies in Table 1, the fitted classical central barrier lies 10.36 kcal/mol below the reactants' classical potential. This fitted classical central barrier is 3.59 and 1.65 kcal/mol higher, respectively, than the QCISD(T) and CCSD(T) classical central barriers (i.e. see Table 1).

V. Discussion

In previous theoretical calculations by Su and co-workers,[23] it was assumed that the $F^- + CH_3Cl$ central barrier has a negligible effect on the substitution rate, and an orientation function was combined with the trajectory capture rate to fit the experimental results. The calculation reported here does not use an explicit orientation function, but it is implicit in the combination of the CH_3Cl angular momentum with the orbital angular momentum to form the total angular momentum.

(56) Hu, W.-P.; Truhlar, D. G. *J. Am. Chem. Soc.* **1995**, *117*, 10726.

However, the orientation effect in this calculation is different from that of Su et al.[23] In their calculation, the largest reaction probability is for collinear ion−molecule collisions, with the probability decreasing with increase of the angle between the dipole vector and the vector connecting F^- with the center-of-mass of CH_3Cl. In the statistical calculation, the orientation effect is determined by two competing processes. At large impact parameters (which implies large orientation angles are more probable) the probability distribution $P(l)$ in eq 7 is large, but the rotational barrier is high at the central barrier, which reduces the probability P_{bran}. The situation is reversed for small impact parameters. Therefore, the net reaction probability reaches a maximum at non-zero impact parameter collisions.

To analyze the effects of energy and angular momenta on the $F^- + CH_3Cl$ S_N2 rate constants, it is helpful to consider the unified statistical model's microcanonical expression

$$k(E,J) = \frac{N^{\ddagger}_{var}(E,J)}{h\rho_{rea}(E,J)} \frac{N^{\ddagger}_{bar}(E,J)}{N^{\ddagger}_{var}(E,J) + N^{\ddagger}_{bar}(E,J) - N^{\ddagger}_{var}(E,J)N^{\ddagger}_{bar}(E,J)/N_{com}(E,J)} \quad (12)$$

where $\rho_{rea}(E,J)$ is the density of states for the reactants $F^- + CH_3Cl$. Even if the central barrier approaches zero and $J = 0$, $N_{com}(E,J)$ will exceed $N^{\ddagger}_{bar}(E,J)$ because of the tighter structure and higher vibrational frequencies at the central barrier. In the following, three limiting cases are considered for $k(E,J)$, with a very low central barrier:

(i) At large E and small J, the variational transition state for capture $N^{\ddagger}_{var}(E,J)$ approaches $N_{com}(E,J)$, $N^{\ddagger}_{var}(E,J) \approx N_{com}(E,J)$. Therefore, eq 12 reduces to

$$k(E,J) = \frac{N^{\ddagger}_{bar}(E,J)}{h\rho_{rea}(E,J)} \quad (13)$$

The expression is essentially the simple microcanonical transition state expression for the "direct" process, i.e., without trapping in the pre-reaction complex and with the central barrier the "bottleneck" for the reactive flux.

(ii) At small E and large J, there is a high rotational energy at the central barrier transition state, and the variational transition state for capture is far from the complex. In this case, both $N^{\ddagger}_{bar}(E,J)$ and $N^{\ddagger}_{var}(E,J)$ are much smaller than $N_{com}(E,J)$. Hence, eq 12 reduces to

$$k(E,J) = \frac{N^{\ddagger}_{var}(E,J)}{h\rho_{rea}(E,J)} \frac{N^{\ddagger}_{bar}(E,J)}{N^{\ddagger}_{var}(E,J) + N^{\ddagger}_{bar}(E,J)} \quad (14)$$

which is essentially the expression for a bimolecular reaction with a long-lived intermediate complex. In this case, the overall substitution rate constant is determined by the capture rate constant times the branching ratio which is not unity. Therefore, the central barrier also plays an important role.

(iii) At small E and very small J ($J \approx 0$), $N^{\ddagger}_{var}(E,J) \ll N^{\ddagger}_{bar}(E,J)$. Equation 12 then reduces to

$$k(E,J) = \frac{N^{\ddagger}_{var}(E,J)}{h\rho_{rea}(E,J)} \quad (15)$$

which is the microcanonical capture rate constant.

As the central barrier height becomes larger, (i) and (ii) above still hold but (iii) does not. This is because, for a large barrier height, $N^{\ddagger}_{bar}(E,J)$ becomes much smaller than $N_{com}(E,J)$ and eq 15 is no longer valid.

The above analysis shows the assumption, that the central barrier has little effect on the rate constant for reaction 2, is probably not correct for most circumstances. In fact, even if the central barrier height is very small, the only case that it is unimportant is for small total energy and very small total angular momentum. As can be seen from the different probability distribution functions in eq 7 and also from classical trajectory calculations for S_N2 reactions, large l collisions, leading to large J, make significant contributions to the S_N2 reactions. According to statistical theory, the low central barrier for a S_N2 reaction affects the rate constant differently than the prediction of the proposed orientation function.[23]

The statistical theory calculations reported here are based on the PES(F,Cl) analytic potential energy function fit to MP2/6-311++G(2df,2pd) *ab initio* calculations. Though they reproduce the overall features of the experimental $k(E_{rel},T)$ curves for the $F^- + CH_3Cl$ S_N2 reaction, quantitative agreement between statistical theory and experiment cannot be attained when using the central barrier height as an adjustable parameter. The statistical theory calculations predict $k(E_{rel},T)$ to decrease with increase in T, while the experiments show no definitive temperature dependence. The calculations only qualitatively reproduce the experimental $k(E_{rel},T)$ curves versus E_{rel}. The best fit to the experimental rates is obtained with a central barrier height larger than that determined from the highest level *ab initio* calculations. Fitting $k(E_{rel},T)$ for $E_{rel} = 0.9$ kcal/mol and $T = 296$ K requires a zero-point corrected central barrier 5.7 kcal/mol higher than the F^-- - -CH_3Cl pre-reaction complex. Using the harmonic frequencies of PES(F,Cl), to remove the barrier/pre-reaction complex zero-point energy difference, lowers this barrier to 5.4 kcal/mol and makes it 10.36 kcal/mol below the reactants' classical potential. In contrast, the MP2, QCISD(T), and CCSD(T) classical barriers are 11.56, 13.95, and 12.01 kcal/mol lower than the reactants' classical potential (see Table 1). The fitted classical barrier of 5.4 kcal/mol, with respect to the pre-reaction complex, is substantially larger than the QCISD(T) and CCSD(T) values of 2.6 and 3.0 kcal/mol, respectively, for this barrier height.

Because of the low central barrier and resulting very short RRKM lifetime of approximately 10^{-13}−10^{-12} second for F^-- - -CH_3Cl complexes formed by $F^- + CH_3Cl$ association, it is very likely that IVR[20] is incomplete for these complexes.[14,57] As a result, a statistical model would be insufficient for describing the kinetics for reaction 2 as found here. The inability of statistical theory to give a complete fit to the $F^- + CH_3Cl$ kinetics does not necessarily implicate a possible microscopic reaction mechanism. As discussed previously,[14] both a direct substitution mechanism and one in which the F^-- - -CH_3Cl complex is formed are possible. A trajectory study for reaction 2 should identify the relative importance of these two mechanisms. The orientation factor proposed by Su et al.[23] may be important[13] for the direct substitution mechanism. For the complex formation mechanism the high-frequency C−H stretching, bending, and rocking modes may be adiabatic, so that energy redistribution only occurs between the low-frequency C−F and C−Cl stretching and bending degrees of freedom. Trajectories would be helpful for testing this model. It would also be interesting to use this model in future statistical theory calculations for reaction 2.

Acknowledgment. This research was supported by the National Science Foundation. The authors wish to thank T. Su, P. Botschwina, and S. Seeger for helpful discussions.

(57) Boering, K. A.; Brauman, J. I. *J. Chem. Phys.* **1992**, *97*, 5439.

Appendix: Statistical Calculation of the Capture Rate

Su[38] used a model atom−rigid rotor Hamiltonian, with the ion-dipole/ion-induced-dipole potential, to determine parametrized trajectory capture rate constants. The Hamiltonian is

$$H = \frac{p_r^{\,2}}{2\mu} + \frac{l^2}{2\mu r^2} + Bj^2 - \frac{\alpha q^2}{2r^4} - \frac{q\mu_D}{r^2}\cos\gamma \qquad \text{(A1)}$$

with

$$\cos\gamma = -\cos q_l \cos q_j + \frac{l^2 + j^2 - J^2}{2lj}\sin q_l \sin q_j \qquad \text{(A2)}$$

where q_l and q_j are the conjugate angular coordinates for l and j. In the initial presentation in this Appendix l, j, and J are used to represent the orbital, rotor rotational, and total angular momenta, respectively. Semiclassical expressions are then used to transform these angular momenta to their associated quantum numbers. This is a standard approach[33] and avoids the confusion of using unconventional symbols for either the angular momenta or their quantum numbers.

For ion−rigid rotor collisions with fixed initial relative translational energy E_{rel} and rotor angular momentum j, the statistical theory constant for ion−rotor capture may be written as[54,58−63]

$$k_{cap}(E_{rel},j) = \frac{N(E_{rel},j)}{2\pi\hbar\rho(E_{rel},j)} \qquad \text{(A3)}$$

where $N(E_{rel},j)$ is the sum of states for the capture variational transition state. The classical density of states (per unit volume) of the separated atom−rigid rotor, $\rho(E_{rel},j)$, is

$$\rho(E_{rel},j) = 2j\frac{\pi}{4\hbar}\left(\frac{8\mu}{4\pi^2\hbar^2}\right)^{3/2} E_{rel}^{\,1/2} \qquad \text{(A4)}$$

As described below, the explicit expression for $N(E_{rel},j)$ depends on the coupling assumed between E_{rel} and j.[39]

1. E_{rel} and j Uncoupled. One model is to treat the relative translational and rigid-rotor motions uncoupled. This may follow, if the capture transition state is very loose and the rigid-rotor motion is essentially a free rotation. Therefore, from the reactants' asymptote to the transition state, there is no energy transfer between the rigid rotor and orbital motions. Similar to phase space theory for the microcanonical case,[54,58] the sum of states $N(E_{rel},j,r)$ at fixed E_{rel} and j and a fixed value for r is a 10-dimensional phase integral for the five degrees of freedom; i.e.

$$N(E_{rel},j,r) = \frac{1}{(2\pi\hbar)^4}\int_0^\infty dl \int_0^\infty dj' \int_{|l-j'|}^{l+j'} dJ \int_{-J}^{J} dJ_z \int_{-\infty}^{\infty} dp_r \int_0^{2\pi} dq_l \int_0^{2\pi} dq_j \int_0^{2\pi} dq_J \int_0^{2\pi} dq_{J_z} \int_0^\infty dr' \frac{dS}{dt} h\left(\frac{dS}{dt}\right) \delta(S)\,\delta(E_{rel} - H_{rel})\,\delta(j' - j) \qquad \text{(A5)}$$

where l, j, J, and J_z are the orbital angular momentum, the rotational angular momentum for rigid rotor, the total angular momentum, and the projection of total angular momentum, respectively. h and δ are the Heaviside step-function and Dirac delta-function, respectively. $S = 0$ is the dividing surface naturally chosen as

$$S = r' - r = 0 \qquad \text{(A6)}$$

and q_l, q_j, q_J, and q_{J_z} are the conjugate coordinates to the above angular momenta. H_{rel} is the Hamiltonian for the relative motion, which is eq A1 with Bj^2 removed.

Below, the above classical expressions for $k_{cap}(E_{rel},j)$ and $N(E_{rel},j,r)$ are transformed to quantum mechanical expressions with the following semiclassical substitutions for the angular momenta;[33] i.e.

$$j \rightarrow (j + {}^1/_2)\hbar, \qquad l \rightarrow (l + {}^1/_2)\hbar, \qquad J \rightarrow (J + {}^1/_2)\hbar \qquad \text{(A7)}$$

where l, j, and J now represent the angular momentum quantum numbers. The density-of-states expression, eq A4, is rewritten as

$$\rho(E_{rel},j) = (2j+1)\frac{\pi}{4}\left(\frac{8\mu}{4\pi^2\hbar^2}\right)^{3/2} E_{rel}^{\,1/2} \qquad \text{(A8)}$$

Using eq A6 and the Hamiltonian for relative translation, six variables of eq A5 may be integrated out. The resulting expression for the sum of states is

$$N(E_{rel},j,r) = \frac{1}{(2\pi)^2}\int_0^{2\pi} dq_l \int_0^{2\pi} dq_j \sum_{l=0}^{\infty}\sum_{J=|l-j|}^{l+j} (2J+1)\, h\left(E_{rel} - \frac{l(l+1)\hbar^2}{2\mu r^2} + \frac{\alpha q^2}{2r^4} + \frac{q\mu_D}{r^2}\cos\gamma\right) \qquad \text{(A9)}$$

Gauss−Legendre quadratures may be applied to the 4-dimensional integral of eq A9, so that the variational method may be used to determine the minimum of the sum-of-states, i.e.

$$N(E_{rel},j) = \min_r [N(E_{rel},j,r)] \qquad \text{(A10)}$$

The evaluation of $N(E_{rel},j,r)$ may be simplified by using spherical polar coordinates,[54] with the relationships

$$l(l+1)\hbar^2 = p_{\theta_1}^2 + p_{\phi_1}^2/\sin^2\theta_1 \qquad \text{(A11a)}$$

$$j(j+1)\hbar^2 = p_{\theta_2}^2 + p_{\phi_2}^2/\sin^2\theta_2 \qquad \text{(A11b)}$$

$$cos\,\gamma = cos(\phi_1 - \phi_2)\sin\theta_1 \sin\theta_2 + cos\,\theta_1 \cos\theta_2 \qquad \text{(A11c)}$$

Equation A5 may then be rewritten as

$$N(E_{rel},j,r) = \frac{1}{(2\pi\hbar)^4}\int d\tau_1 \int d\tau_2 \int_{-\infty}^{\infty} dp_r \int_0^{\infty} dr' \frac{dS}{dt} h\left(\frac{dS}{dt}\right)\delta(S)\,\delta(E_{rel} - H_{rel})\,\delta(j'-j) = \frac{1}{(2\pi\hbar)^4}\int d\tau_1 \int d\tau_2\, h(E_{rel} - H_1)\,\delta[j - j(p_{\theta_2}, p_{\phi_2}, \phi_2)] \qquad \text{(A12)}$$

where

$$H_1 = \frac{l(l+1)\hbar^2}{2\mu r^2} + V(r,\cos\gamma) \qquad \text{(A13a)}$$

$$d\tau_1 = dp_{\theta_1}\, dp_{\phi_1}\, d\theta_1\, d\phi_1 \qquad \text{(A13b)}$$

(58) Chesnavich, W. J.; Bowers, M. T. *J. Chem. Phys.* **1976**, *66*, 2306.
(59) Chesnavich, W. J.; Bowers, M. T. *J. Phys. Chem.* **1979**, *83*, 900.
(60) Klippenstein, S. J. *J. Chem. Phys.* **1996**, *104*, 5437.
(61) Smith, S. C.; McEwan, M. J.; Gilbert, R. G. *J. Phys. Chem.* **1989**, *93*, 8143.
(62) Smith, S. C.; Troe, J. *J. Chem. Phys.* **1992**, *97*, 5451.
(63) Chen, Y.; Rauk, A.; Tschulkow-Roux, E. *J. Phys. Chem.* **1991**, *95*, 9900.

$$d\tau_2 = dp_{\theta_2}\, dp_{\phi_2}\, d\theta_2\, d\phi_2 \quad \text{(A13c)}$$

Inserting another delta-function in eq A12, one has

$$N(E_{rel},j,r) = \frac{1}{(2\pi\hbar)^4}\int d\tau_1 \int d\tau_2 \int_{-1}^{1} dz\ \delta[z - z(\theta_1,\theta_2,\phi_1,\phi_2)]\, h(E_{rel} - H_1)\ \delta[j - j(p_{\theta_2},p_{\phi_2},\phi_2)] \quad \text{(A14)}$$

where

$$z(\theta_1,\theta_2,\phi_1,\phi_2) = \cos(\phi_1 - \phi_2)\sin\theta_1 \sin\theta_2 + \cos\theta_1\cos\theta_2 \quad \text{(A15)}$$

Thus, the integration of (A14) may be reduced to

$$N(E_{rel},j,r) = \frac{j+1}{\hbar^2}\mu r^2 \int_{-1}^{1} dz [E_{rel} - V(r,z)] h[E_{rel} - V(r,z)] \quad \text{(A16)}$$

with

$$V(r,z) = -\frac{\alpha q^2}{2r^4} - \frac{\mu_D q}{r^2} z \quad \text{(A17)}$$

The final result is

$$N(E_{rel},j,r) = \frac{2\mu(2j+1)}{\hbar^2}\mu_D q\left(E_{rel} + \frac{\alpha q^2}{2r^4}\right), \quad \text{for } E_{rel} + \frac{\alpha q^2}{2r^4} > \frac{\mu_D q}{r^2} \quad \text{(A18a)}$$

$$= \frac{(2j+1)\mu r^2}{2\hbar^2}\left(E_{rel} + \frac{\alpha q^2}{2r^4} + \frac{\mu_D q}{r^2}\right)^2, \quad \text{for } E_{rel} + \frac{\alpha q^2}{2r^4} \le \frac{\mu_D q}{r^2} \quad \text{(A18b)}$$

The variational transition state and its sum of states $N(E_{rel},j)$ are obtained by taking the derivative of $N(E_{rel},j,r)$ with respect to r and setting it to zero. For $N(E_{rel},j,r)$ in eq A18b, the variational value for r is similar to the definition of the capture radius;[54]

$$r^* = (\alpha q^2/2E_{rel})^{1/4} \quad \text{(A19)}$$

However, if eq A18a is applicable instead of eq A18b, the variational transition state is at infinite separation.

2. E_{rel} and j Strongly Coupled. The second model assumes there is strong coupling between relative translation and rotation so that a microcanonical ensemble is formed for these motions at the transition state. This may follow if the capture transition state is very tight, at which there is extensive energy transfer between the orbital motion and the rigid rotor's rotation. The microcanonical sum of states is

$$N(E,r) = \frac{1}{(2\pi\hbar)^4}\int_0^\infty dj' \int_0^\infty dl \int_{|l-j'|}^{l+j'} dJ \int_{-J}^{J} dJ_z \int_{-\infty}^{\infty} dp_r \int_0^{2\pi} dq_j \int_0^{2\pi} dq_{J_z} \int_0^{2\pi} dq_{j'} \int_0^{2\pi} dq_l \int_0^\infty dr' \frac{dS}{dt} h\left(\frac{dS}{dt}\right) \delta(S)\ \delta(E - H) \quad \text{(A20)}$$

with total energy

$$E = E_{rel} + Bj^2 \quad \text{(A21)}$$

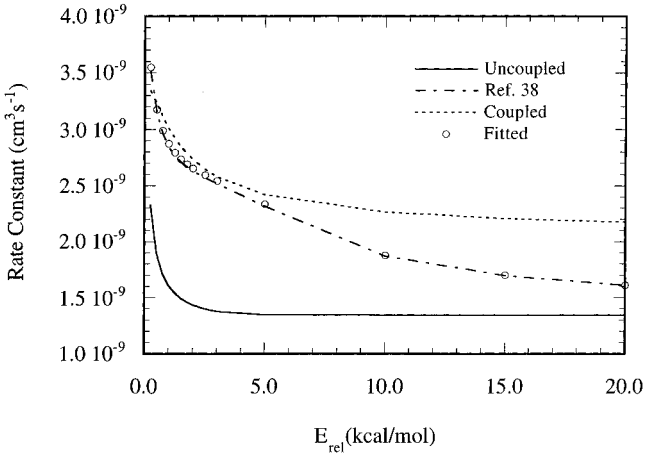

Figure 3. Capture rate constants versus relative translational energy E_{rel} at $T = 300$ K. The uncoupled, coupled, and empirical fitted models are described in the Appendix.

Table 6. Fitting Parameters for Capture Rate Constant[a]

E_{rel} (kcal/mol)	$A(E_{rel})$	$B(E_{rel})$
0.25	2.85189557	0.0356277041
0.50	2.98278785	0.0324389338
0.75	3.01673961	0.0306278300
1.00	3.01158333	0.0291165095
1.25	3.00127196	0.0280265529
1.50	2.98277831	0.0270502400
1.75	2.95650768	0.0261207949
2.00	2.92512298	0.0252334438
2.50	2.85501146	0.0236322712
3.00	2.77168322	0.0221119318
5.00	2.36031246	0.0162640009
10.00	1.60009110	0.00652402779
15.00	1.39846778	0.00459949812
20.00	1.29862380	0.00349968974

[a] The parameters are defined in the Appendix and are unitless.

Again, spherical polar coordinates may be used[54] and the final simplified result is

$$N(E,r) = \frac{\mu r^2 I}{\hbar^4}\int_{-1}^{1} dz\ [E - V(r,z)]^2\ h[E - V(r,z)] \quad \text{(A22)}$$

where I is the moment of inertia for the diatomic rigid rotor. Analytic solutions to eq A22 are found for the two different conditions similar to those in eqs A18a and A18b [i.e., replace E_{rel} with E in those conditions]. The variational transition state and its sum of states $N(E)$ are found from the minimum in $N(E,r)$ versus r.

This $N(E)$ is the total sum of states for energy E. However, what is needed in eq A3 is $N(E_{rel},j)$, which is the part of $N(E)$ which arises from the reactants with relative translational energy E_{rel} and rotational angular momentum number j. This is equal to

$$N(E_{rel},j) = N(E)P(E_{rel},j) \quad \text{(A23)}$$

where $P(E_{rel},j)$ is the flux of reactants with E_{rel} and j divided by the total reactant flux at energy E. Since the flux is proportional to the number of states,[33] this flux ratio is simply eq A16 divided by eq A22, evaluated at the limit $r \to \infty$. The potential $V(r,z)$ in eqs A16 and A22 is zero for $r \to \infty$ and

$$P(E_{rel},j) = \frac{(2j+1)E_{rel}}{E^2 I/\hbar^2} \quad \text{(A24)}$$

Values of $k_{cap}(E_{rel},j)$ for the above two models; i.e. E_{rel} and j uncoupled or strongly coupled, were then inserted into eq 6 to determine $k_{cap}(E_{rel},T)$. The nature of the resulting rate constants and their comparison with Su's parametrized trajectory rate constants are shown in Figure 3 for $T = 300$ K. The uncoupled E_{rel} and j model underestimates Su's rate constants. While Su's rate constants are overestimated by the strongly coupled model,[64] this model gives rate constants in agreement with those of Su's at low E_{rel}. At high E_{rel}, the uncoupled model is in better agreement with Su's parametrized capture rates.

For the statistical analyses reported here, it is assumed Su's $k_{cap}(E_{rel},T)$ are correct. Thus, to obtain the $k_{cap}(E_{rel},j)$ for eq 7, consistent with Su's $k_{cap}(E_{rel},T)$, the uncoupled $k_{cap}(E_{rel},j)$ were scaled by $A(E_{rel})e^{-B(E_{rel})j}$ so that when inserted into eq 6 they gave Su's $k_{cap}(E_{rel},T)$. The resulting fit is shown in Figure 3 for $T = 300$ K. The fitting parameters are listed in Table 6.

JA962622J

(64) At low E_{rel} and T, the strongly coupled E_{rel} and j statistical rate constants are smaller than Su's parametrized trajectory capture rate constants. This is because there is still an appreciable interaction between the ion and dipole at the initial separation of 50 Å used in the trajectory calculations, which affects the capture dynamics at small E_{rel} and T; e.g., see ref 13.